Towards enhanced mobility of exploration space rovers with trailing arm suspension: An investigative approach

A F. Baza[1] , A M. Ali[2] , and E Said[3]

[1] Defense Research Center, Egyptian Armed Forces
[2] Automotive Engineering Department, Military Technical
[3] Mechatronics Engineering Department, Military Technical

E-mail: ahmed.baza57@gmail.com

Abstract. This paper presents a novel study of the handling characteristics in space rovers operating on rough terrains. The proposed approach implements a detailed mathematical model comprising individual rigid bodies, force elements, and suspension mechanisms of the rover. The proposed work is focused on correlated dynamics of the suspension mechanism considering adjustable and tuneable design parameters. To this aim, a set of arbitrary operating conditions, namely, static loading, step-input, and irregular road profiles, are defined to investigate the influence of each parameter on ride comfort, rover agility, and stability of the suspension mechanism. The main contribution of this study can be pointed out as highlighting the mist significantly-influencing design parameters and defining correlated break-points for the rover design, to adjust and tune the dynamic response of the suspension system according to the characteristics of irregular terrains. Moreover, the proposed work provides scholars and researchers with a user-friendly benchmark for further analysis and optimal design attempts of space rovers.

1. Background

A significant potential has been put to explore the possibility of life on near planets using space rovers, for instance the Apollo LRV missions in the 1970s and many more modern studies [1, 2]. In this context, agile unmanned ground vehicles are indispensable to conduct sample collection and terrain exploration mission after space-crafts' landing [3, 4]. Wheeled rovers capable of moving on off-road terrains claimed a lot of success in recent years during interplanetary expeditions that used to carry astronauts to space whether on the surface of the Moon or Mars [5, 6].

At the present stage of technology, wheeled space rovers still offer many advantages, in particular, are concerned with reliability, energy consumption, and ease of control [7, 8]. In planetary rovers, operations on unsuitable and irregular terrains is a design perquisite to ensure durability and avoid unnecessary falling of assigned mission [9, 10]. Hence, rovers must be equipped with state-of-the-art

technology that allows them to traverse over highly rugged and uneven terrain [11, 12]. In this regard, optimal design of vehicle undercarriage is a milestone to yield desired mobility and robustness of the rover [13].

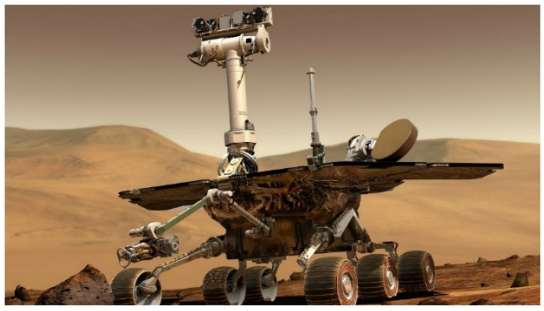

Figure 1. A wheeled space rover for terrain exploration missions [14].

Significant advances in space rover suspension systems has been introduce in literature by considering ride comfort as a main objective in addition to reduce wheel load variations below body structure resonances [6, 15]. Furthermore, lightweight and flexible of the suspension system gained a lot of attention as design goal to ensures that all rover-wheels are in permanent contact with the ground during terrain traversing [16, 17]. This latter aspect is key-factor for vehicular stability and maneuverability and to provide smooth running on unpaved environments [18].

In light thereof, many suspension mechanisms have been studied to increase the agility, robustness, and stability of space rovers, such as swing axle, double wishbone, Macpherson strut, trailing arm, and others [19-21]. Independent suspension systems have been increasingly considered for space rovers due to the ability of such suspension system to support wheel load robustly and enable vertical movement of the un-sprung mass without affecting other undercarriage systems. To this aim, this paper is focused on investigating the multiple privileges of such rover suspension systems based on proper modelling of a trailing arm quarter space rover model (QSRM) and conducting an investigative approach to explore most influencing design parameters pseudo-condition approach [22-24].

2. A multiple-degree-of-freedom model of QSRM

2.1. Modelling concept and detailed parameters of QSRM

The presented QSRM in figure 2, includes rover body and a trailing-arm connection jointing the knuckle and rover wheels [23, 25]. A trailing arm is connected to a revolute center (B) considering arm's rotation. The knuckle described by the angle (β), which is affected by a torsional spring damper connection [26, 27]. The wheel rotation is denoted by (φ) [25]. For further detailed about adopted model in this work, the reader is referred to [28].

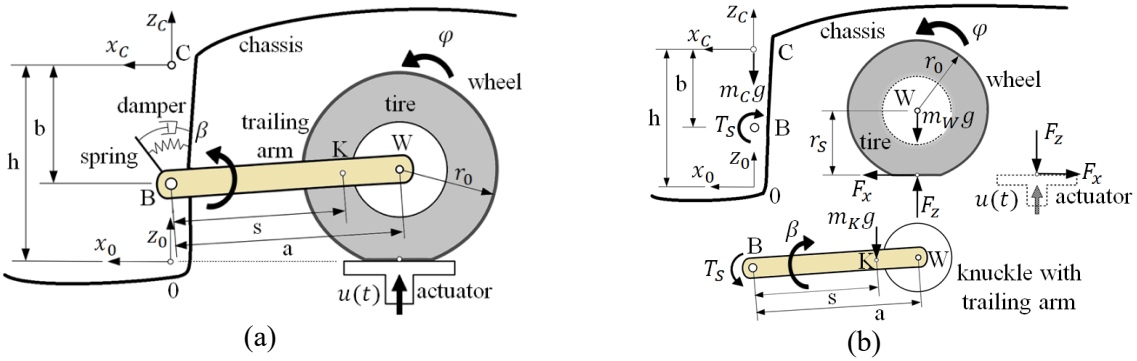

Figure 2. Illustration of QSRM using trailing arm suspension (a) and detailed individual rigid bodies, applied forces, and torques (b) – re-drawn based on published works of [23].

2.2. Kinematical relations of the QSRM

The kinematic relation of presented QSRM can be formulated considering $y = [z \;\; \beta \;\; \varphi]$, whereby

$$r_{0-c0} = \begin{bmatrix} 0 \\ 0 \\ h+z \end{bmatrix}, \quad v_{0-c0} = \begin{bmatrix} 0 \\ 0 \\ \dot{z} \end{bmatrix}, \text{ and } a_{0-c0} = \begin{bmatrix} 0 \\ 0 \\ \ddot{z} \end{bmatrix}. \tag{1}$$

The coordinates transformation of the trailing arm and the knuckle can be conducted through

$$A_{C-K} = \begin{bmatrix} \cos\beta & 0 & \sin\beta \\ 0 & 1 & 0 \\ -\sin\beta & 0 & \cos\beta \end{bmatrix}, \tag{2}$$

whereby

$$\omega_{0-K,0} = \begin{bmatrix} 0 \\ 1 \\ 0 \end{bmatrix} \dot{\beta} \qquad \text{and} \qquad \alpha_{0-K0} = \begin{bmatrix} 0 \\ 1 \\ 0 \end{bmatrix} \ddot{\beta}. \tag{3}$$

The position vector of knuckle trailing arm center is defined as

$$r_{0-K0} = \begin{bmatrix} 0 \\ 0 \\ h+z \end{bmatrix} + \begin{bmatrix} 0 \\ 0 \\ -b \end{bmatrix} + \begin{bmatrix} -s\cos\beta \\ 0 \\ s\sin\beta \end{bmatrix}, \tag{4}$$

whereto the time derivatives can be obtained as

$$v_{0-K0} = \begin{bmatrix} 0 \\ 0 \\ 1 \end{bmatrix} \dot{z} + \begin{bmatrix} s\sin\beta \\ 0 \\ s\cos\beta \end{bmatrix} \dot{\beta}, \tag{5}$$

for which, the acceleration will be:

$$a_{0-K0} = \begin{bmatrix} 0 \\ 0 \\ 1 \end{bmatrix} \ddot{z} + \begin{bmatrix} s\sin\beta \\ 0 \\ s\cos\beta \end{bmatrix} \ddot{\beta} + \begin{bmatrix} s\cos\beta \\ 0 \\ -s\sin\beta \end{bmatrix} \dot{\beta}^2 \tag{6}$$

The transformation matrix for W can be given by [29]

$$A_{0-W} = \begin{bmatrix} \cos\varphi & 0 & \sin\varphi \\ 0 & 1 & 0 \\ -\sin\varphi & 0 & \cos\varphi \end{bmatrix}, \tag{7}$$

resulting in the formulation

$$\omega_{0-W0} = \begin{bmatrix} 0 \\ 1 \\ 0 \end{bmatrix} \dot{\varphi}, \qquad \alpha_{0-W0} = \begin{bmatrix} 0 \\ 1 \\ 0 \end{bmatrix} \ddot{\varphi}, \tag{8}$$

$$v_{0-W0} = \begin{bmatrix}0\\0\\1\end{bmatrix}\dot{z} + \begin{bmatrix}a\ sin\beta\\0\\a\ cos\beta\end{bmatrix}\dot{\beta}, \text{ and} \tag{9}$$

$$a_{0-W0} = \begin{bmatrix}0\\0\\1\end{bmatrix}\ddot{z} + \begin{bmatrix}a\ sin\beta\\0\\a\ cos\beta\end{bmatrix}\ddot{\beta} + \begin{bmatrix}a\ cos\beta\\0\\-a\ sin\beta\end{bmatrix}\dot{\beta}^2. \tag{10}$$

2.3. Kinetic aspects and the equation of motion of the proposed QSRM

The total affecting torque about the joint in B can be formulated as

$$T_s = -(T_S^0 + c_S\beta + d_S\dot{\beta}), \tag{11}$$

where T_S^0 is the spring preload, c_S the spring rate, and d_S is the damper constant. The forces excreting on rover wheels are hence modelled as

$$F_z = c_z(r_0 - r_S) \tag{12}$$

whereby the tractive effort will be

$$F_x = -c_x(a(1-\cos\beta) - (h+z-b+a\sin\beta-u)\varphi) - d_x\big(a\sin\beta\,\dot{\beta} - (h+z-b+a\sin\beta-u)\dot{\varphi}\big). \tag{13}$$

The differential equations describing the motion of presented QSRM under the aforementioned forces and kinematical relations can be formulated for $\dot{y} = z$ and $M\,\dot{z} = q$ [30]

where y denotes the vector of generalized coordinates, the vector z defines trivial generalized velocities, and the mass matrix M is defined by these relations

$$M = \begin{bmatrix} m_C + m_K + m_W & (s\,m_K + a\,m_W)\cos\beta & 0\\ (s\,m_K + a\,m_W)\cos\beta & \Theta_K + s^2\,m_K + a^2\,m_W & 0\\ 0 & 0 & \Theta_W\end{bmatrix} \quad \text{and} \tag{14}$$

$$q = \begin{bmatrix} F_z - (m_C + m_K + m_W)\,\mathrm{g} + (s\,m_K + a\,m_W)\sin\beta\,\dot{\beta}^2\\ T_S - (s\,m_K + a\,m_W)\cos\beta\,g + a(F_x\sin\beta + F_z\cos\beta)\\ -r_S\,F_x\end{bmatrix}. \tag{15}$$

2.3.1. Steady-state conditions under rover's weight

The influencing forces under steady-state conditions are simplified to

$$T_s \to T_S^{st} = -(T_S^0 + c_S\beta^{st}), \tag{16}$$

leading to the reduced formulas

$$F_z - (m_C + m_K + m_W)\,\mathrm{g} = 0, \tag{17}$$

$$-\big(T_S^0 + c_S\beta^{st}\big) - s_S m_S\cos\beta^{st}\,g + a\big({F_x}^{st}\sin\beta^{st} + {F_z}^{st}\cos\beta^{st}\big) = 0, \text{ and} \tag{18}$$

$$-r_S{F_x}^{st} = 0, \tag{19}$$

where the steady-state tire forces become

$${F_z}^{st} = (m_C + m_K + m_W)\,\mathrm{g} \quad \text{and} \quad {F_x}^{st} = 0, \tag{20}$$

Entailing an initial static angle (β_{st})

$$-\big(T_S^0 + c_S\beta_{st}\big) - s_S m_S\cos\beta_{st}\,g + a(F_x^{st}\sin\beta_{st} + F_z^{st}\cos\beta_{st}) = 0 \tag{21}$$

2.3.2. Dynamic input to the QSRM considering random road profile

Road profiles for QSRM terrain can be characterized by the measurement of elevation profiles via high-speed profilometers or point-by-point measurements [27, 31, 32]. As depicted in figure 3 [33], the power-spectral-density (psd) can be used to approximate random road profiles as

$$\Phi(\Omega) = \Phi(\Omega_0)\left(\frac{\Omega}{\Omega_0}\right)^{-\omega} \tag{22}$$

where the wavenumber and PSD are denoted by $\Omega = 2\pi/L$ and $\Phi_0 = \Phi(\Omega_0)$ respectively. For an arbitrary value of waviness to $\omega = 2$, different classes of road profile can be assigned.

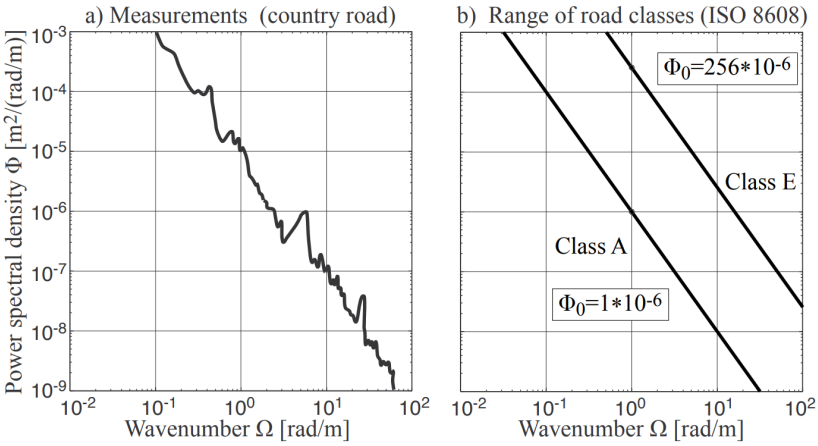

Figure 3. Measured and categorized rated PSD for different roads [23].

A single track's profile can be hence modelled as

$$z_R(s) = \sum_{i=1}^{N} A_i \sin(\Omega_i\, s + \Psi_i), \tag{23}$$

whereby, the amplitude is given as

$$A_i = \sqrt{2\,\Phi(\Omega_i)\Delta\Omega}\,, \qquad i = 1(1)N, \tag{24}$$

as depicted for a finite horizon with N-equal intervals $\Delta\Omega = \frac{\Omega_N - \Omega_1}{N}$.

3. Theoretical simulation and correlation

3.1. Steady-state behavior

The steady state behaviour can be observed in figure 5 for the static angle (β_{st}), which behaves inversely w.r.t. preload torsion, in contrast to a proportional relation with the torsional spring rate (c_S). On the other side, the increasing rate in β_{st} has been found proportional to the trailing arm's length at low torsional spring rate (c_S), which can be illustrated by the two slopes in figure 5(b).

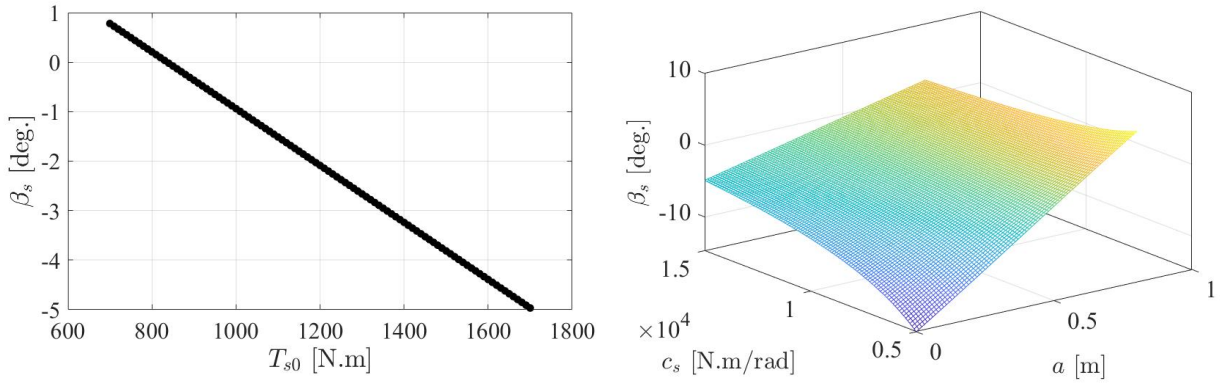

(a) (b)

Figure 4. Correlation between the static angle (β_{st}) with the preload in torsion (T_S^0) (a) and with both torsional spring rate (c_S) and the length of the trailing arm (knuckle) (b)

3.2. The influence of a step input and pseudo road profile on the rover

The dynamic step response of QSRM is illustrated in Figure 6. For a step input with the characteristics $t_{step} = 0.75\ [s]$ and $u_{step} = 0.05\ [m]$, it can be observed that the vertical displacement is inversely proportional to the torsional damper constant (d_S) until a break-point value at ($d_S = 870\ [N.m.s]$, $z = 0.0917\ [m]$) then this effect inverses. Hence, the inverse proportionality of the angle (β) with the damper constant (d_S) can be perceived. On the other side, the displacement (z) and the spring rate (c_S) are related with a characteristic break-point at ($c_S = 10800\ [N.m/rad]$, $z = 0.0917\ [m]$), at which the influence becomes adverse.

For further analysis of the correlation between design parameters, the vertical displacement (z) is characterized with a proportional response related to the spring rate (c_S) at high torsional damper constant (d_S), which is greater than that at low torsional damper constant (d_S) that is illustrated by the two slopes in figure 7. The similar observation is noted for the knuckle static angle (β), which increases by the increment of the spring rate (c_S) and the damper constant (d_S).The static angle (β) increases proportionally to the knuckle length starting from ($a \cong 0.2\ [m]$ approximately) but concerning the torsional damper constant (d_S) is approximately constant (no observable change).

There are some essential parameters that should be considered in order to describe a pseudo random road profile, they are provided in the subsequent table:

Table 1. Model parameter of arbitrary road profile for QRM with trailing arm [23, 34].

Physical quantities	Symbols	Values	Units
Wave number	Ω	-	$[rad/m]$
Power-spectral-density	Φ_0	1×10^{-6}	$[m^2/(rad/m)]$
Waviness	ω	2	$unitless$
Phase lag between the left and right tracks	Ψ	-	$[rad.]$
Local friction coefficient (Tire/road friction coefficient)	μ	1	$unitless$
Rover velocity	v	22.222	$[m/s]$

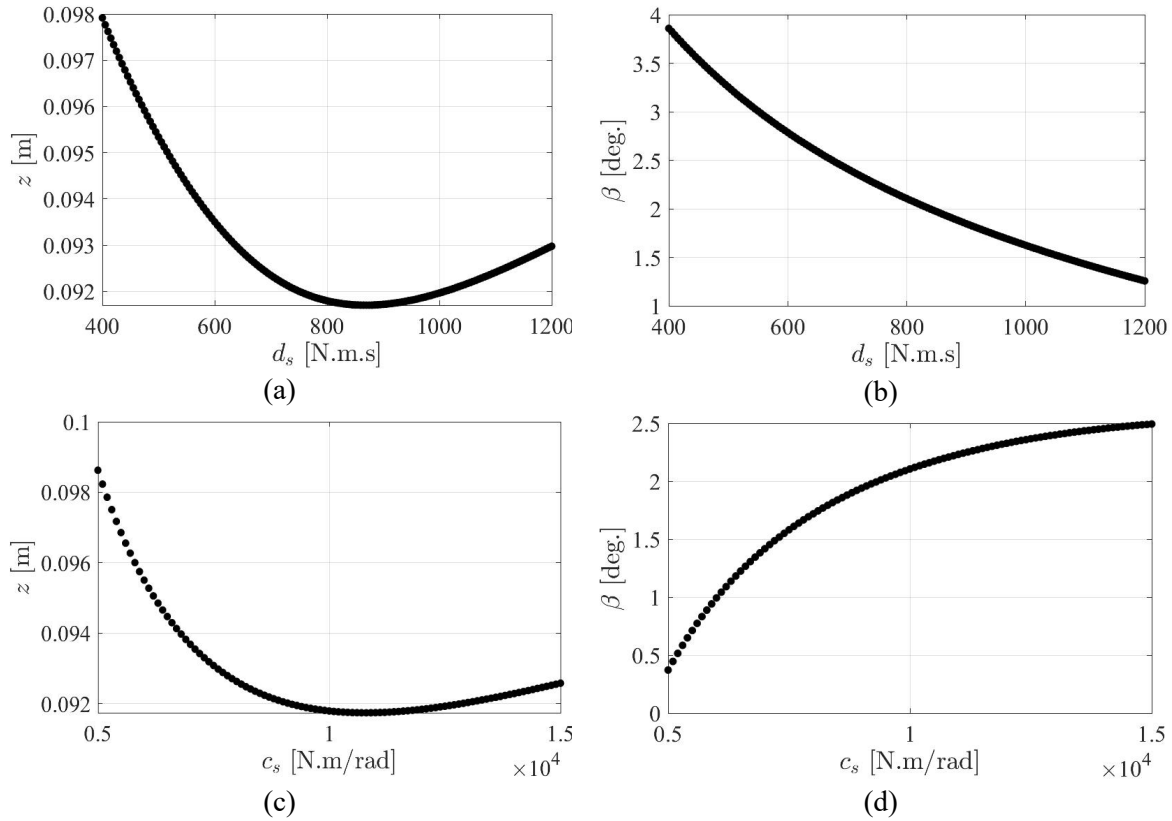

Figure 5. Dynamic characteristics of the step response for proposed QSRM

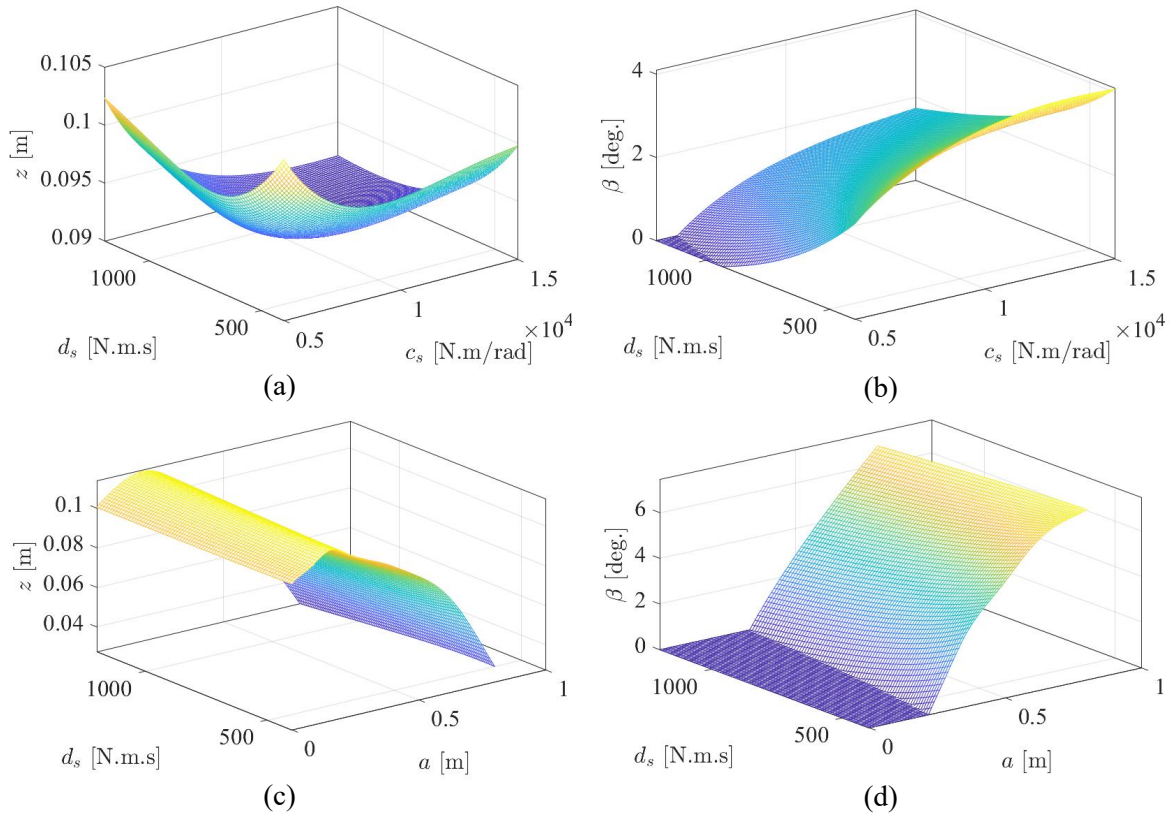

Figure 6. Correlated step response characteristics of the proposed QSRM

The pseudo random road profile can be simulated according to the above-mentioned relations and the results are shown in figures 8 and 9. A significant proportionality between (β) and (z_C) with the road waviness and PSD can be observed. However, the same relation with road waviness is characterized with a particular break-point at ($\omega = 2.5, \beta = -0.48712\ [deg.]$) then this effect is strongly reversed.

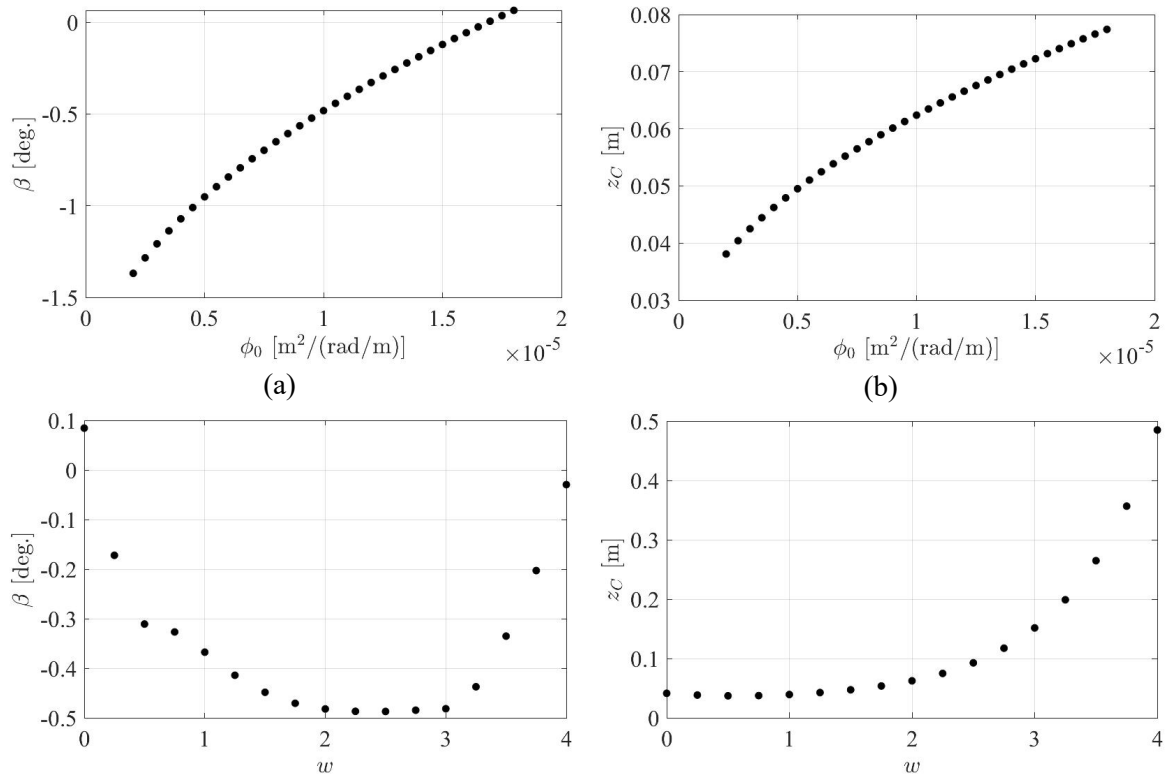

Figure 7. Dynamic behavior of QSRM considering different PSD of the road

On the other side, the static angle (β) is merely proportional to the road PSD, yet concerning the waviness of road (ω) is approximately constant (no observable change) as illustrated in Figure 9. The displacement (z_C) is approximately constant (no observable change) at low waviness of road (ω). Furthermore, the force (F_z) rises a little at low waviness of road (ω) but is approximately constant (no observable change) at high waviness of road (ω).

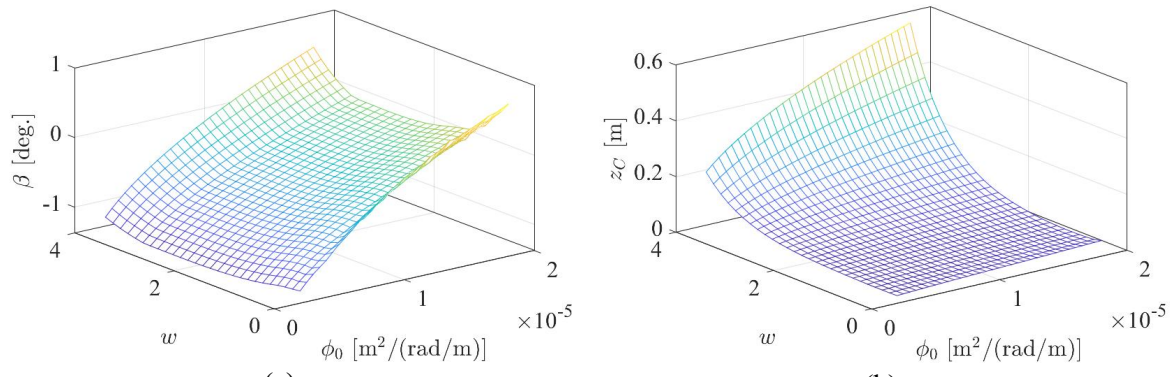

Figure 8. Correlated of the dynamic behavior of QSRM considering different PSD of the road

4. Analysis of results and discussion

4.1. Insights into the behavior of individual design parameters

In light of given analysis and illustrations of QSRM response under different operating conditions, it can be out forth that the dynamic behavior of such suspension mechanism can be improved by tuning various significant parameters, such as the knuckle's length and the damping ratio (d_s) to obtain appropriate tunable values for (β) and (z), as follows: First, the influence of the knuckle static angle at steady state (β_{st}), with a step and the displacement (z). Second, the spring rate (c_s) influences the knuckle static angle at (β_{st}), with a step input for (z). Finally, the damping constant (d_s) influences the knuckle static angle with step input (β), considering optimal behavior of the displacement (z).

4.2. Generalized break-points for optimal suspension design

It can be systematically perceived from the behavioral analysis in figures 10 and 11 that the angle (β_{st}) has a typical proportional response with the depicted parameters, but it only reflects at ($a = 0.56\ [m]$ and $\beta_{st} = 0.0295551\ [deg.]$);considering arbitrary values of (c_s). However, the displacement (z) decreases by the increment of (a) while the torsional damper constant (d_s) is approximately irrelevant in this case (no observable change).

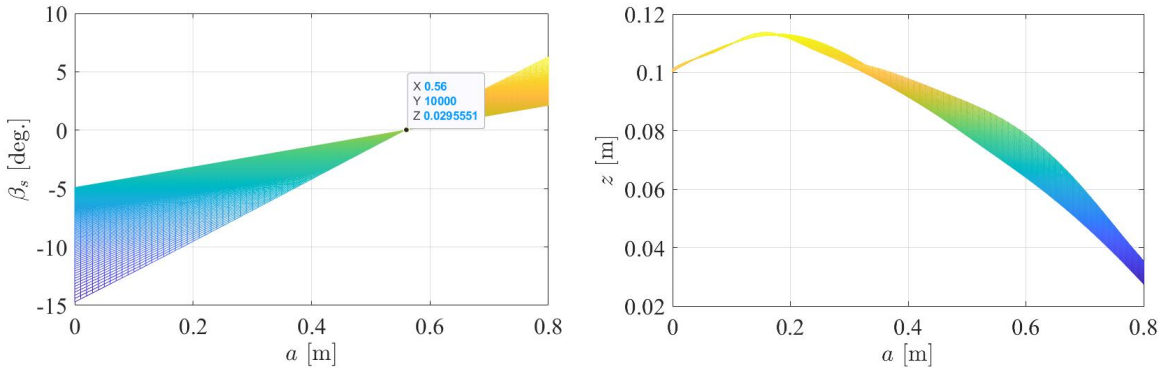

(a) (b)

Figure 9. Generalized break-points for optimal design and ride characteristics of QSRM

While the static angle (β) increases related to the knuckle length (a) starting from ($a \cong 0.2\ [m]$ approximately) whereas the torsional damper constant (d_s) is approximately constant (no observable change). Therefore, it can be concluded from the previous demonstrated simulation that, regardless the values of (c_s) and (d_s) are, the knuckle length (a) is always equal to $0.56\ [m]$ and the initial angle (β_{st}) invariably equals to $0.0295551\ [deg.]$.

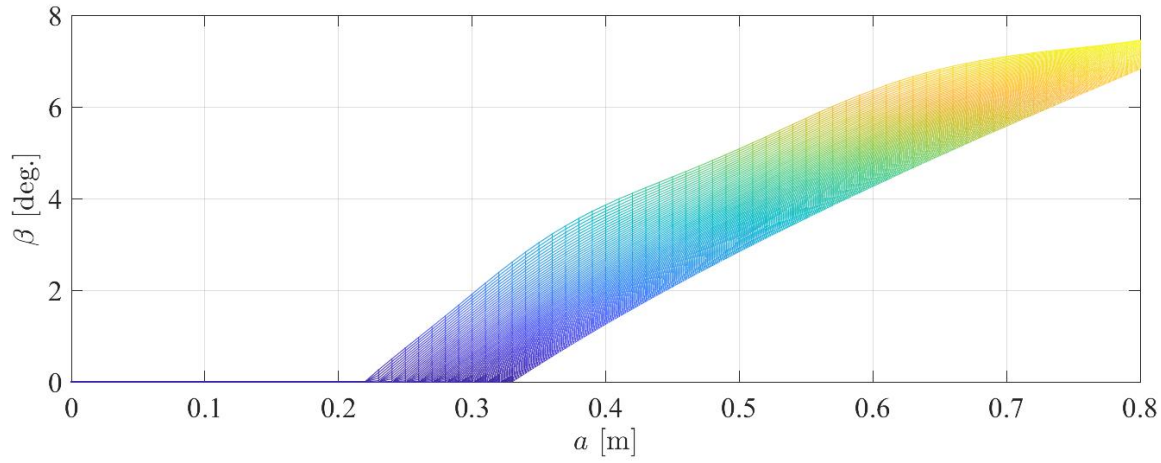

Figure 10. Generalized break-points for the angle (β) by the increment of knuckle center distance

5. Conclusion and future work

This study proposed a systematic approach to develop a validated rover suspension model, considering the dynamic response to step input and road irregularities. The developed rover suspension mechanism enables detailed insights into the interrelated behaviors and dynamics of each component to ensure operational robustness, dynamic stability, and agility over different terrains. In this regard, it has been demonstrated that the knuckle length of the suspension system, the spring rate, and the damping constant have more impact than other parameters on the rover's characteristics such as the arm's angle and the vertical setting of the rover. Consequently, the main contribution of this research is to point out major bear-points of the rover design, including trailing arm angle and the vertical setting of the rover via tuning of the knuckle length and the spring rate, whereto the damping constant is also adjusted to obtain an appropriate suspension system for the rover.

References

[1] Chen, F. and G. Genta, *Dynamic modeling of wheeled planetary rovers: A model based on the pseudo-coordiates approach*. Acta Astronautica, 2012. **81**(1): p. 288-305.

[2] Ali, A.M., R. Shivapurkar, and D. Soeffker. *Development and improvement of a situation-based power management method for multi-source electric vehicles*. in *2018 IEEE Vehicle Power and Propulsion Conference (VPPC)*. 2018. IEEE.

[3] Schenker, P.S., et al., *Planetary rover developments supporting mars exploration, sample return and future human-robotic colonization*. Autonomous Robots, 2003. **14**(2): p. 103-126.

[4] Balme, M., et al., *UK Space Agency "Mars Utah Rover Field Investigation 2016"(MURFI 2016): Overview of Mission, Aims and Progress*. 2017.

[5] Jain, A., et al. *Recent developments in the ROAMS planetary rover simulation environment*. in *2004 IEEE aerospace conference proceedings (IEEE Cat. No. 04TH8720)*. 2004. IEEE.

[6] Schenker, P.S. *Advances in rover technology for space exploration*. in *2006 IEEE Aerospace Conference*. 2006. IEEE.

[7] Wang, J., et al., *Dynamic modeling and vibration analysis for the vehicles with rigid wheels based on wheel-terrain interaction mechanics*. Shock and Vibration, 2015. **2015**.

[8] Asfoor, M.S. and A.M. Ali. *Energy-efficient electrification of public transportation fleets based on generic driving cycles for the city of Cairo, Egypt*. in *2021 IEEE Vehicle Power and Propulsion Conference (VPPC)*. 2021. IEEE.

[9] Cordes, F., et al. *An active suspension system for a planetary rover*. in *Proceedings of the International Symposium on Artificial Intelligence, Robotics and Automation in Space (i-SAIRAS)*. 2014.

[10] M. Ali, A. and D. Söffker. *Realtime application of progressive optimal search and adaptive dynamic programming in multi-source HEVs*. in *Dynamic Systems and Control Conference*. 2017. American Society of Mechanical Engineers.

[11] Zhou, F., et al., *Simulations of mars rover traverses*. Journal of Field Robotics, 2014. **31**(1): p. 141-160.

[12] Shibly, H., *Analysis of the effect of soft soil's parameters change on planetary vehicles' dynamic response*. Journal of Automation Mobile Robotics and Intelligent Systems, 2017. **11**.

[13] Maurette, M., *Mars rover autonomous navigation*. Autonomous Robots, 2003. **14**(2): p. 199-208.

[14] India TV News Desk. *Watch stunning first ever 4K video from Mars surface shot by 3 NASA rovers*. 2020 5 January 2023]; Available from: https://www.indiatvnews.com/science/mars-surface-4k-video-released-watch-space-exloration-videos-photos-from-mars-nasa-rover-636440.

[15] Sharp, R. and D. Crolla, *Road vehicle suspension system design-a review*. Vehicle system dynamics, 1987. **16**(3): p. 167-192.

[16] Karnopp, D., *Active damping in road vehicle suspension systems*. Vehicle System Dynamics, 1983. **12**(6): p. 291-311.

[17] Aly, A.A. and F.A. Salem, *Vehicle suspension systems control: a review*. International journal of control, automation and systems, 2013. **2**(2): p. 46-54.
[18] Ali, A.M., R. Shivapurkar, and D. Söffker, *Optimal situation-based power management and application to state predictive models for multi-source electric vehicles*. IEEE Transactions on Vehicular Technology, 2019. **68**(12): p. 11473-11482.
[19] Zahir, E., et al. *6 Wheeled Mars rover design for terrain traversing, equipment servicing, astronaut assistance and on-board testing*. in *2016 IEEE/SICE International Symposium on System Integration (SII)*. 2016. IEEE.
[20] Bastow, D., G. Howard, and J.P. Whitehead, *Car suspension and handling*. 2004: SAE international Warrendale.
[21] Qi, Y., et al., *RESEARCH ON TRAILING ARM SUSPENSION SYSTEM OF FULL X-BY-WIRE CONTROL CHASSIS BASED ON DATA DRIVE*. 力学学报, 2022. **54**(5): p. 1-16.
[22] Gao, B., et al., *Control of a hydropneumatic active suspension based on a non-linear quarter-car model*. Proceedings of the Institution of Mechanical Engineers, Part I: Journal of Systems and Control Engineering, 2006. **220**(1): p. 15-31.
[23] Rill, G., *Road vehicle dynamics: fundamentals and modeling*. 2011: Crc Press.
[24] Ali, A.M. and B. Moulik, *On the role of intelligent power management strategies for electrified vehicles: A review of predictive and cognitive methods*. IEEE Transactions on Transportation Electrification, 2021. **8**(1): p. 368-383.
[25] Gipser, M. *FTire, a new fast tire model for ride comfort simulations*. in *International ADAMS User's Conference Berlin*. 1999.
[26] Ukamnal, S., et al., *Design of Trailing Arm Suspension*. International Journal of Engineering Research, 2014. **3**(6).
[27] Banerjee, S., V. Balamurugan, and R. Krishnakumar, *Ride comfort analysis of math ride dynamics model of full tracked vehicle with trailing arm suspension*. Procedia Engineering, 2016. **144**: p. 1110-1118.
[28] Rill, G., et al., *Leaf spring modeling for real time applications*. The Dynamics of Vehicles on Road and on Tracks–Extensive Summaries, IAVSD, 2003. **3**.
[29] Rill, G., *A modified implicit Euler algorithm for solving vehicle dynamic equations*. Multibody System Dynamics, 2006. **15**(1): p. 1-24.
[30] Kane, T.R. and D.A. Levinson, *Formulation of equations of motion for complex spacecraft*. Journal of Guidance and control, 1980. **3**(2): p. 99-112.
[31] Dhir, A. and S. Sankar, *Dynamics of off-road tracked vehicles equipped with trailing arm suspension*. Proceedings of the Institution of Mechanical Engineers, Part D: Journal of Automobile Engineering, 1995. **209**(3): p. 195-215.
[32] Ali, A.M. and M.I. Yacoub. *Optimal predictive power management strategy for fuel cell electric vehicles using neural networks in real-time*. in *2020 IEEE Vehicle Power and Propulsion Conference (VPPC)*. 2020. IEEE.
[33] Butz, T., M. Ehmann, and T.-M. Wolter, *A realistic road model for real-time vehicle dynamics simulation*. 2004, SAE Technical Paper.
[34] Rill, G. and A.A. Castro, *Road vehicle dynamics: fundamentals and modeling with MATLAB®*. 2020: CRC Press.